

Variational study of Fermi-surface deformations in Hubbard models

JÖRG BÜNEMANN¹, TOBIAS SCHICKLING² and FLORIAN GEBHARD²

¹ *Institut für Physik, BTU Cottbus, D-03013 Cottbus, Germany*

² *Fachbereich Physik, Philipps Universität Marburg, D-35032 Marburg, Germany*

PACS 71.10.Fd – Lattice fermion models

Abstract – We study the correlation-induced deformation of Fermi surfaces by means of a new diagrammatic method which allows for the analytical evaluation of Gutzwiller wave functions in finite dimensions. In agreement with renormalization-group results we find Pomeranchuk instabilities in two-dimensional Hubbard models for sufficiently large Coulomb interactions.

Introduction. – The shape of the Fermi surface (FS) is one of the most important properties that determine the low-energy physics of electron liquids. The single-particle energy levels of non-interacting electrons depend on the crystal momentum \mathbf{k} from the Brillouin zone through the (single-band) dispersion relation $\varepsilon(\mathbf{k})$. For N electrons at zero temperature, all single-particle states which lie below the Fermi energy E_F are occupied. The FS separates occupied and unoccupied single-particle levels, i.e., it consists of all \mathbf{k} -points which obey the equation $E_F - \varepsilon(\mathbf{k}_F) = 0$. In the presence of finite Coulomb interactions, the calculation of the FS requires the real part of the proper self-energy $\Sigma(\mathbf{k}, \omega)$ so that the FS is obtained from

$$E_F - \varepsilon(\mathbf{k}_F) - \Re \Sigma(\mathbf{k}_F, E_F) = 0. \quad (1)$$

Within perturbation theory for the Coulomb interaction [1], the proper self-energy is defined as the sum over all irreducible diagrams for the single-particle Green function.

The calculation of $\Sigma(\mathbf{k}, \omega)$ is a notoriously difficult task in correlated-electron theory, even for a single-band Hubbard model

$$\hat{H} = \hat{H}_0 + U \sum_{\mathbf{i}} \hat{d}_{\mathbf{i}}, \quad \hat{H}_0 = \sum_{\mathbf{i}, \mathbf{j}, \sigma} t_{\mathbf{i}, \mathbf{j}} \hat{c}_{\mathbf{i}, \sigma}^\dagger \hat{c}_{\mathbf{j}, \sigma}, \quad \hat{d}_{\mathbf{i}} \equiv \hat{n}_{\mathbf{i}, \uparrow} \hat{n}_{\mathbf{i}, \downarrow} \quad (2)$$

in two dimensions. Here, $\mathbf{i} = (i_1, i_2)$ denotes one of the L sites on a square lattice, and $\sigma = \uparrow, \downarrow$. The dispersion relation is given by

$$\varepsilon(\mathbf{k}) = \frac{1}{L} \sum_{\mathbf{i}, \mathbf{j}} \exp[i(\mathbf{i} - \mathbf{j})\mathbf{k}] t_{\mathbf{i}, \mathbf{j}}. \quad (3)$$

For small U , the self-energy $\Sigma(\mathbf{k}, \omega)$ may be calculated from straightforward perturbation theory [2–4], or using renormalisation-group methods [5, 6]. When U is of the order of the bare bandwidth W , or larger, only purely numerical methods such as Quantum-Monte Carlo [7, 8] and Exact Diagonalisation [9] are available which still suffer from serious finite-size limitations [9, 10]. In view of these significant problems on the theoretical side, our understanding of experiments on two-dimensional Fermi surfaces, e.g., those of doped cuprates, is far from satisfactory. Moreover, only reliable many-particle approaches permit a meaningful comparison of measured and calculated Fermi surfaces that may reveal the correct form of \hat{H}_0 in (2); for a recent overview, see, e.g., Ref. [9].

In this work, we introduce a new analytical scheme to evaluate expectation values for Gutzwiller wave functions in *finite* spatial dimensions in a controlled way. By construction, the Gutzwiller approach provides the Fermi surface of quasi-particles in Landau’s Fermi-liquid theory. Therefore, the Gutzwiller wave function is an appropriate tool for the calculation of correlation-induced FS deformations at moderate interaction strengths, $U \approx W$. Unlike numerical schemes for the evaluation of Gutzwiller wave functions [11–15] our approach does not suffer from finite-size limitations. It therefore provides us with a momentum-space resolution that is needed for the study of Fermi-surface deformations.

Evaluation of Gutzwiller wave functions. – The variational wave functions introduced by Gutzwiller [16] for the single-band Hubbard model (2) have the form

$$|\Psi_G\rangle = \hat{P}_G |\Psi_0\rangle = \prod_{\mathbf{i}} \hat{P}_{\mathbf{i}, G} |\Psi_0\rangle, \quad (4)$$

where $|\Psi_0\rangle$ is a (normalised) single-particle product state and the local ‘Gutzwiller correlator’ is defined by

$$\hat{P}_{\mathbf{i};G} = 1 - (1 - g)\hat{d}_{\mathbf{i}}. \quad (5)$$

Here, $g \geq 0$ is a variational parameter which allows for the optimisation of the average number of doubly-occupied lattice sites. In this work, we will use the more convenient definition

$$\hat{P}_{\mathbf{i}} = \sum_{\Gamma} \lambda_{\Gamma} |\Gamma\rangle_{\mathbf{i}} \langle \Gamma| \quad (6)$$

for the local correlator. It contains the variational parameters λ_{Γ} for the four local states

$$|\Gamma\rangle_{\mathbf{i}} \in \{|\emptyset\rangle_{\mathbf{i}}, |\uparrow\rangle_{\mathbf{i}}, |\downarrow\rangle_{\mathbf{i}}, |\uparrow\downarrow\rangle_{\mathbf{i}}\} \quad (7)$$

for the empty, singly, or doubly occupied site \mathbf{i} . To keep notations simple, we assume that the wave functions $|\Psi_G\rangle$ and $|\Psi_0\rangle$ are translationally invariant and paramagnetic. The corresponding derivation for more general wave functions is straightforward.

In order to determine the expectation value of the Hamiltonian (2) with respect to the wave function (4) we need to evaluate ($\mathbf{i} \neq \mathbf{j}$)

$$\langle \Psi_G | \Psi_G \rangle = \left\langle \prod_{\mathbf{i}} \hat{P}_{\mathbf{i}}^2 \right\rangle_0, \quad (8)$$

$$\langle \Psi_G | \hat{d}_{\mathbf{i}} | \Psi_G \rangle = \left\langle \hat{P}_{\mathbf{i}} \hat{d}_{\mathbf{i}} \hat{P}_{\mathbf{i}} \prod_{\mathbf{l}(\neq \mathbf{i})} \hat{P}_{\mathbf{l}}^2 \right\rangle_0, \quad (9)$$

$$\langle \Psi_G | \hat{c}_{\mathbf{i},\sigma}^{\dagger} \hat{c}_{\mathbf{j},\sigma} | \Psi_G \rangle = \left\langle \tilde{c}_{\mathbf{i},\sigma}^{\dagger} \tilde{c}_{\mathbf{j},\sigma} \prod_{\mathbf{l}(\neq \mathbf{i}, \mathbf{j})} \hat{P}_{\mathbf{l}}^2 \right\rangle_0, \quad (10)$$

where $\langle \dots \rangle_0$ denotes expectation values with respect to $|\Psi_0\rangle$ and $\tilde{c}_{\mathbf{i},\sigma}^{(\dagger)} \equiv \hat{P}_{\mathbf{i}} \hat{c}_{\mathbf{i},\sigma}^{(\dagger)} \hat{P}_{\mathbf{i}}$. As we will show below, our diagrammatic expansion significantly simplifies if we set

$$\hat{P}_{\mathbf{i}}^2 = 1 + x \hat{d}_{\mathbf{i}}^{\text{HF}}, \quad (11)$$

where

$$\hat{d}_{\mathbf{i}}^{\text{HF}} \equiv \hat{n}_{\mathbf{i},\uparrow}^{\text{HF}} \hat{n}_{\mathbf{i},\downarrow}^{\text{HF}}, \quad \hat{n}_{\mathbf{l},\sigma}^{\text{HF}} \equiv \hat{n}_{\mathbf{l},\sigma} - n_0, \quad (12)$$

and $n_0 \equiv \langle \hat{n}_{\mathbf{l},\sigma} \rangle_0 = N/(2L)$. Equation (11) determines three of the four parameters λ_{Γ} as well as the coefficient x . In this way, we are left with only one variational parameter. For instance, we may express the parameters λ_{\emptyset} , $\lambda_{\uparrow} \equiv \lambda_{\sigma}$ for empty and singly-occupied sites by λ_d , the parameter for doubly-occupied sites. Alternatively, due to the relations

$$x = [\lambda_d^2 - 1]/(1 - n_0)^2 \Leftrightarrow \lambda_d^2 = 1 + x(1 - n_0)^2, \quad (13)$$

we may also consider x as our variational parameter. The expansion (11) was first introduced in Ref. [17] where it has been used as a convenient tool for the evaluation of expectation values in infinite dimensions $D = \infty$ and of $1/D$ corrections. For another series expansion for the Gutzwiller wave function around the limit $D = \infty$, see Ref. [18]. Note that both local correlators $\hat{P}_{\mathbf{i};G}$ and $\hat{P}_{\mathbf{i}}$,

together with the condition (11), lead to the same variational space if the single-particle wave function $|\Psi_0\rangle$ is treated as a variational object.

With Eq. (11), the norm and the expectation values Eqs. (8)–(10) are given in form of a power series in x ,

$$\langle \Psi_G | \Psi_G \rangle = \sum_{k=0}^{\infty} \frac{x^k}{k!} \sum'_{\mathbf{l}_1, \dots, \mathbf{l}_k} \langle \hat{d}_{\mathbf{l}_1, \dots, \mathbf{l}_k}^{\text{HF}} \rangle_0, \quad (14)$$

$$\langle \Psi_G | \hat{d}_{\mathbf{i}} | \Psi_G \rangle = \lambda_d^2 \sum_{k=0}^{\infty} \frac{x^k}{k!} \sum'_{\mathbf{l}_1, \dots, \mathbf{l}_k} \langle \hat{d}_{\mathbf{i}} \hat{d}_{\mathbf{l}_1, \dots, \mathbf{l}_k}^{\text{HF}} \rangle_0, \quad (15)$$

$$\langle \Psi_G | \hat{c}_{\mathbf{i},\sigma}^{\dagger} \hat{c}_{\mathbf{j},\sigma} | \Psi_G \rangle = \sum_{k=0}^{\infty} \frac{x^k}{k!} \sum'_{\mathbf{l}_1, \dots, \mathbf{l}_k} \langle \tilde{c}_{\mathbf{i},\sigma}^{\dagger} \tilde{c}_{\mathbf{j},\sigma} \hat{d}_{\mathbf{l}_1, \dots, \mathbf{l}_k}^{\text{HF}} \rangle_0, \quad (16)$$

where we introduced the notation

$$\hat{d}_{\mathbf{l}_1, \dots, \mathbf{l}_k}^{\text{HF}} \equiv \hat{d}_{\mathbf{l}_1}^{\text{HF}} \dots \hat{d}_{\mathbf{l}_k}^{\text{HF}}, \quad \hat{d}_{\emptyset}^{\text{HF}} \equiv 1. \quad (17)$$

The primes in Eqs. (14)–(16) indicate the summation restrictions $\mathbf{l}_p \neq \mathbf{l}_{p'}$, $\mathbf{l}_p \neq \mathbf{i}, \mathbf{j}$ for all p, p' . Note that the same expressions arise for the original Gutzwiller correlator $\hat{P}_{\mathbf{i};G}$ when we replace x and $\hat{d}_{\mathbf{l}}^{\text{HF}}$ by $(g^2 - 1)$ and $\hat{d}_{\mathbf{l}}$, respectively [19, 20]. As we will demonstrate below, our expansion with respect to x converges significantly faster than the expansion in $(g^2 - 1)$. Therefore, the first few orders in the x -expansion permit us to evaluate the Gutzwiller wave function accurately for not too large interaction strengths.

The expectation values in Eqs. (14)–(16) can be evaluated by means of Wick’s theorem [1]. By construction, we eliminated all diagrams with local ‘Hartree bubbles’ at internal vertices. To achieve the same for the external vertices we rewrite the corresponding operators in Eqs. (15), (16) as

$$\hat{d}_{\mathbf{i}} = (1 - x d_0) \hat{d}_{\mathbf{i}}^{\text{HF}} + n_0 (\hat{n}_{\mathbf{i},\uparrow}^{\text{HF}} + \hat{n}_{\mathbf{i},\downarrow}^{\text{HF}}) + d_0 \hat{P}_{\mathbf{i}}^2, \quad (18)$$

$$\tilde{c}_{\mathbf{i},\sigma}^{(\dagger)} = \hat{P}_{\mathbf{i}} \hat{c}_{\mathbf{i},\sigma}^{(\dagger)} \hat{P}_{\mathbf{i}} = q \hat{c}_{\mathbf{i},\sigma}^{(\dagger)} + \alpha \hat{c}_{\mathbf{i},\sigma}^{(\dagger)} \hat{n}_{\mathbf{i},\bar{\sigma}}^{\text{HF}}, \quad (19)$$

where we introduced

$$d_0 \equiv n_0^2, \quad (20)$$

$$q \equiv \lambda_1 (\lambda_d n_0 + \lambda_{\emptyset} (1 - n_0)), \quad (21)$$

$$\alpha \equiv \lambda_1 (\lambda_d - \lambda_{\emptyset}), \quad (22)$$

and $\bar{\uparrow} = \downarrow$, $\bar{\downarrow} = \uparrow$. When inserted into (15), the last term in (18) combines to $\lambda_d^2 d_0 \langle \Psi_G | \Psi_G \rangle$ so that it does not have to be evaluated diagrammatically. In the resulting diagrammatic expansion of Eqs. (14)–(16), the k th-order terms correspond to diagrams with k ‘internal’ vertices on sites $\mathbf{l}_1, \dots, \mathbf{l}_k$, one (two) ‘external’ vertices on site \mathbf{i} (\mathbf{i} and \mathbf{j}) and lines

$$P_{\mathbf{l},\mathbf{l}'}^{\sigma} \equiv \langle \hat{c}_{\mathbf{l},\sigma}^{\dagger} \hat{c}_{\mathbf{l}',\sigma} \rangle_0 - \delta_{\mathbf{l},\mathbf{l}'} n_0 \quad (23)$$

connecting these vertices.

As the final analytical step of our derivation, we apply the linked-cluster theorem [1]. The norm (14) cancels

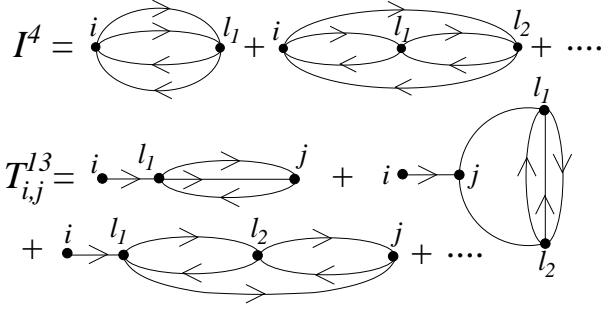


Fig. 1: Diagrams with up to two internal vertices for $I^{(4)}$ and $T_{i,j}^{(1),(3)}$.

the disconnected diagrams in the two denominators (15) and (16). Note that a straightforward application of this theorem is hampered by the summation restrictions in these equations. However, applying Wick's theorem to the expectation values in (14)–(16) is equivalent to the evaluation of determinants such as $|P_{1,l'}^\sigma|$ with $\mathbf{l}, \mathbf{l}' \in \{\mathbf{l}_1, \dots, \mathbf{l}_k\}$. Since these determinants vanish if any of the lattice sites $\mathbf{l}_1, \dots, \mathbf{l}_k$ are the same, we can lift the summation restrictions in (14)–(16) without creating additional terms.

The remaining task is to evaluate the six diagrammatic sums

$$S = \sum_{k=0}^{\infty} \frac{x^k}{k!} S(k) \quad (24)$$

with

$$S \in \{I^{(2)}, I^{(4)}, T^{(1),(1)}, T^{(1),(3)}, T^{(3),(1)}, T^{(3),(3)}\} \quad (25)$$

and

$$I^{(2)[(4)]}(k) \equiv \sum_{\mathbf{l}_1, \dots, \mathbf{l}_k} \langle \hat{n}_{i,\sigma}^{\text{HF}} [\hat{d}_{i,\sigma}^{\text{HF}}] \hat{d}_{\mathbf{l}_1, \dots, \mathbf{l}_k}^{\text{HF}} \rangle_0^c, \quad (26)$$

$$T_{i,j}^{(1)[(3)],(1)[(3)]}(k) \equiv \sum_{\mathbf{l}_1, \dots, \mathbf{l}_k} \langle [\hat{n}_{i,\sigma}^{\text{HF}}] \hat{c}_{i,\sigma}^\dagger [\hat{n}_{j,\sigma}^{\text{HF}}] \hat{c}_{j,\sigma} \hat{d}_{\mathbf{l}_1, \dots, \mathbf{l}_k}^{\text{HF}} \rangle_0^c.$$

Here, $\langle \dots \rangle_0^c$ indicates that only connected diagrams are to be kept. As examples, we show the leading order diagrams of $I^{(4)}$ and $T_{i,j}^{(1),(3)}$ in Fig. 1.

The variational ground-state energy functional is given by

$$\langle \hat{H} \rangle_{\text{G}} = E_0(|\Psi_0\rangle, x) = L(E^{\text{kin}} + Ud) \quad (27)$$

in the form

$$\begin{aligned} \langle \hat{H} \rangle_{\text{G}} = & 2 \sum_{i,j} t_{i,j} (q^2 T_{i,j}^{(1),(1)} + 2q\alpha T_{i,j}^{(1),(3)} + \alpha^2 T_{i,j}^{(3),(3)}) \\ & + LU \lambda_d^2 ((1-xd_0)I^{(4)} + 2n_0 I^{(2)} + d_0), \end{aligned} \quad (28)$$

where $|\Psi_0\rangle$ enters the energy expression solely through the lines $P_{i,j}^\sigma$ and through n_0 . In our case of a translationally invariant wave function, we have

$$\langle \hat{n}_{i,\sigma} \rangle_{\text{G}} = n_0. \quad (29)$$

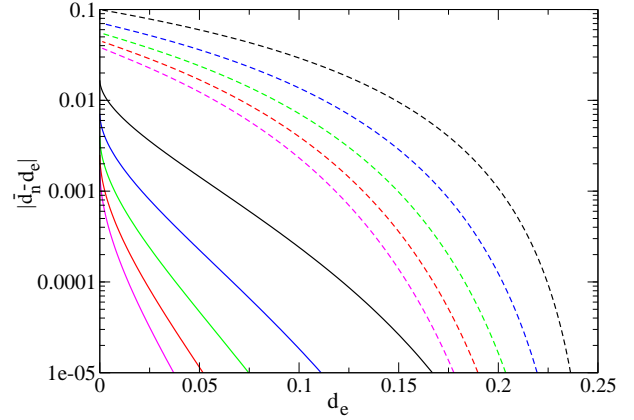


Fig. 2: Difference between the exact double occupancy d_e and its n -th order Taylor expansions \bar{d}_n (with $n = 3, 5, 7, 9, 11$ in one dimension (in descending order) with expansion parameter x (solid line) and $(g^2 - 1)$ (dashed line).

The l.h.s. of (29) is given diagrammatically as

$$\begin{aligned} \langle \hat{n}_{i,\sigma} \rangle_{\text{G}} = & \lambda_d^2 (d_0 + I^{(4)}(1 - xd_0) + 2n_0 I^{(2)}) \\ & + \lambda_1^2 (m_1^0 + I^{(2)}(1 - 2n_0) - I^{(4)}(1 + x)m_1^0), \end{aligned} \quad (30)$$

where $m_1^0 = n_0(1 - n_0)$. From (29), (30), (13), and

$$\lambda_1^2 = 1 - n_0(1 - n_0)x, \quad (31)$$

we then find the following relation between $I^{(4)}$ and $I^{(2)}$,

$$I^{(2)} = -I^{(4)} \frac{x(1 - 2n_0)}{1 + xn_0(1 - n_0)}. \quad (32)$$

Therefore, only $I^{(4)}$ in (28) needs to be calculated.

The one-dimensional Hubbard model. – We have tested the quality of our x -expansion against the exact results for the Gutzwiller wave function in one dimension [19, 20]. From the analytical results one can, e.g., determine the Taylor expansions of the average double occupancy with respect to x or $(g^2 - 1)$ [21]. It turns out that the x -expansion converges much faster than the expansion in $(g^2 - 1)$. This can be seen, for example, in Fig. 2 where the differences between the exact double occupancy (d_e) and its n -th order Taylor expansions (\bar{d}_n) at half band-filling ($n_0 = 1/2$) are shown for both parameters as a function of d_e . The figure reveals that the x -expansion to third order is by an order of magnitude closer to the exact result than the 11th-order expansion in $(g^2 - 1)$.

In order to assess the absolute quality of our diagrammatic x -expansion, we prefer to define the ‘order’ of the expansion by the number of internal vertices which we retain in the diagrams. Consequently, the corresponding expressions for the kinetic energy E_k^{kin} and the double occupancy d_k to k th order are *not* identical to the k th order Taylor expansions because the coefficients q , α , λ_d also depend on x . In Fig. 3 we show the deviations of the results to leading orders ($k \leq 4$) for the kinetic energy

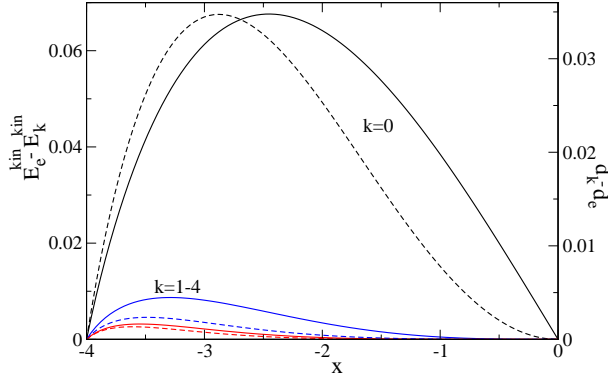


Fig. 3: Differences between the exact double occupancy d_e (right axis) and kinetic energy E_e^{kin} (left axis) within the Gutzwiller wave function in one dimension at half band-filling [19, 20] and the corresponding k th order diagrammatic results for the double occupancy d_k (solid lines, $n = 0, 1, 3$, in descending order) and the kinetic energy E_k^{kin} (dashed lines, $k = 0, 2, 4$, in descending order).

and the double occupancy from the analytic results in one dimension at half band-filling ($n_0 = 1/2$) as a function of x ($x = -4$ corresponds to the atomic limit $d = 0$). At half band-filling the lowest-order results ($k = 0$) are equivalent to the Gutzwiller approximation [17, 19] because $\alpha(n_0 = 1/2) = 0$. Moreover, the even (odd) orders $k > 0$ vanish for the double occupancy (kinetic energy). Fig. 3 shows that the 4th-order results reproduce the exact results very well.

The one-dimensional Hubbard model is the worst case for our formalism because the latter is exact for the Gutzwiller wave function in the opposite limit of infinite dimensions $D = \infty$ where all diagrams vanish. Therefore, we expect that the 4th-order results for the Gutzwiller wave function in two dimensions, which we discuss in the following, are also quite accurate.

Fermi-surface deformations in two-dimensional Hubbard models. – For the two-dimensional Hubbard model, we treat $|\Psi_0\rangle$ and its FS as variational quantities. The minimisation of (28) with respect to $|\Psi_0\rangle$ leads to the effective single-particle equation

$$\hat{H}_0^{\text{eff}}|\Psi_0\rangle = \sum_{\mathbf{i}, \mathbf{j}} t_{\mathbf{i}, \mathbf{j}}^{\text{eff}} \hat{c}_{\mathbf{i}, \sigma}^\dagger \hat{c}_{\mathbf{j}, \sigma} |\Psi_0\rangle = E^{\text{eff}}|\Psi_0\rangle, \quad (33)$$

$$t_{\mathbf{i}, \mathbf{j}}^{\text{eff}} = \frac{\partial E_0(|\Psi_0\rangle, x)}{\partial P_{\mathbf{i}, \mathbf{j}}^\sigma}. \quad (34)$$

The effective dispersion relation

$$\varepsilon^{\text{eff}}(\mathbf{k}) = \frac{1}{L} \sum_{\mathbf{i}, \mathbf{j}} \exp^{i(\mathbf{i}-\mathbf{j})\mathbf{k}} t_{\mathbf{i}, \mathbf{j}}^{\text{eff}} \quad (35)$$

defines the quasi-particle FS via

$$\varepsilon^{\text{eff}}(\mathbf{k}_F) = E_F \quad (36)$$

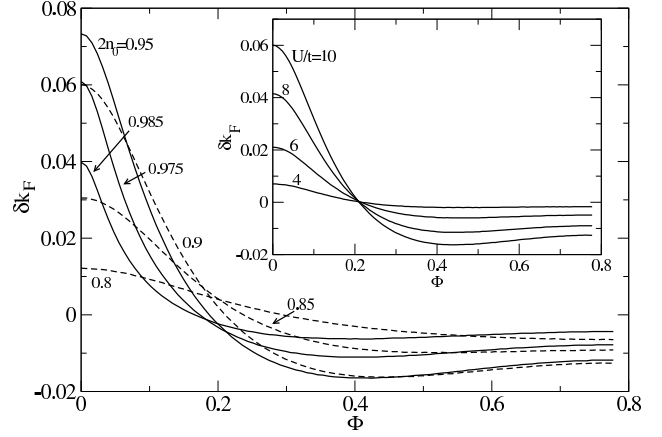


Fig. 4: Polar plot of the FS deformations δk_F for $U/t = 10$ and various band fillings $2n_0$; Inset: FS deformations δk_F for $2n_0 = 0.9$ and various values of U/t .

because the correlated momentum distribution

$$n_{\mathbf{k}, \sigma} \equiv \langle \hat{c}_{\mathbf{k}, \sigma}^\dagger \hat{c}_{\mathbf{k}, \sigma} \rangle_G \quad (37)$$

has step discontinuities exactly at the momenta given by Eq. (36).

The remaining problem is to solve self-consistently the closed set of equations (27), (28), (33)-(36), together with

$$\frac{\partial}{\partial x} E_0(|\Psi_0\rangle, x) = 0. \quad (38)$$

Note that E^{eff} is just an auxiliary quantity, the ground-state energy of the effective single-particle Hamiltonian \hat{H}_0^{eff} . It must not be confused with the variational ground-state energy (28). Numerically, we determine $|\Psi_0\rangle$ by solving (33) in momentum space while the diagrammatic sums in (28) and the derivatives in (34) are evaluated in position space (up to 4th order in this work). For example, in a paramagnetic state, the first two contributions of I^4 in Fig. 1 are given by

$$I^4 = x \sum_{l_1} P_{i, l_1}^4 + 4 \frac{x^2}{2} \sum_{l_1, l_2} P_{i, l_1}^2 P_{i, l_2}^2 P_{l_1, l_2}^2 + \dots \quad (39)$$

where the lines (23) were assumed to be spin independent, $P_{i, j} \equiv P_{i, j}^\sigma$. Note that the combinatorial factor 4 in (39) results from the different possibilities to label the lines with spin indices σ . We have determined these factors by means of a computer algorithm because their calculation becomes quite involved for higher-order diagrams. In this context, it was particularly helpful to use the exact results in one dimension to eliminate programming errors.

In principle, the effective hopping parameters $t_{\mathbf{i}, \mathbf{j}}^{\text{eff}} \equiv t_{X, Y}^{\text{eff}}$ have to be calculated for arbitrary distances $X \equiv i_1 - j_1$, $Y \equiv i_2 - j_2$ of the lattice vectors $\mathbf{i} = (i_1, i_2)$ and $\mathbf{j} = (j_1, j_2)$. However, since the calculation of the derivatives in (34) is numerically quite expensive, we take into account only the dominant parameters $t_{X, Y}^{\text{eff}}$. In our calculations we include the seven hopping parameters with

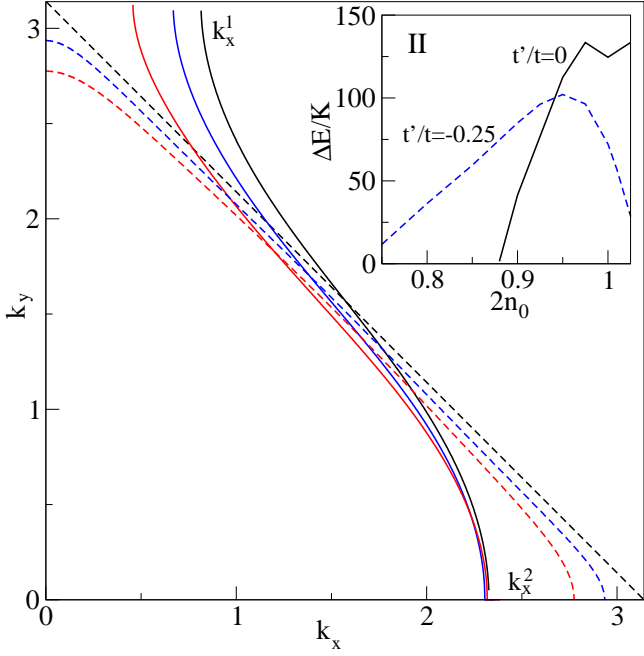


Fig. 5: Pomeranchuk FS for the Hubbard model with nearest-neighbour hopping $t_{1,0} = -t$ for $U/t = 10$ (solid) in comparison with the FS for $U/t = 0$ (dashed) for $2n_0 = 1.0, 0.95, 0.9$ (from right to left). Inset: energy gain ΔE in Kelvin ($t = 1.0$ eV) in the symmetry-broken phase as a function of the filling $2n_0$ for $U/t = 10$.

$X^2 + Y^2 \leq 10$. To be consistent, we also set $P_{X,Y}^\sigma = 0$ for all $X^2 + Y^2 > 10$ in the energy functional $E_0(|\Psi_0\rangle, x)$. This simplifies the numerical evaluation of the diagrams and it ensures that the self-consistency equations (34) lead to a (local) minimum of $E_0(|\Psi_0\rangle, x)$. Note that the numerical calculation of all diagrammatic sums in (28) takes less than a minute on a present-day desktop computer. Once evaluated, the variational ground-state energy can be calculated immediately for *any* value of U . This illustrates that the study of more complicated wave functions or multi-band models in two (or even three) dimensions is a feasible problem within our approach.

We first consider a Hubbard model with only nearest-neighbour hopping $t_{1,0} = -t$ on a square lattice. Since in this case the FS deformations $\delta k_F \equiv k_F(U) - k_F(0)$ are rather small we plot them in a polar diagram as a function of the angle $\Phi = \arctan(k_y/k_x)$. Due to the symmetry of the lattice, we only need to consider angles $\Phi \in (0, \pi/4)$. In Fig. 4 we show δk_F as a function of Φ for various hole-dopings $2n_0 < 1$ near half filling. Due to particle-hole symmetry, it is sufficient to study hole dopings and the FS is unchanged at half band-filling. At finite doping, the overall feature of the FS deformation has a maximum for $2n_0 \approx 0.95$ and it becomes negligible for densities $2n_0 < 0.75$. Note that the Φ -dependence of δk_F is a non-trivial function of the doping. For example, the two curves with $2n_0 = 0.9$ and $2n_0 = 0.975$ have almost the same deformation at $\Phi = 0$ (i.e., in $[0,1]$ direction)

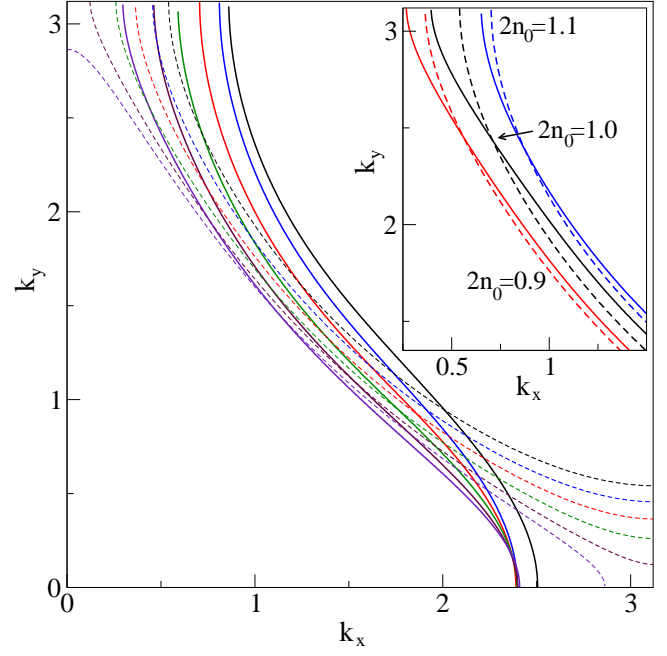


Fig. 6: Pomeranchuk FS for the Hubbard model with nearest-neighbour hopping $t_{1,0} = -t$ and second-neighbour hopping $t_{1,1} = -t' = 0.25t$ for $U/t = 10$ (solid) in comparison with the FS for $U/t = 0$ (dashed) for $2n_0 = 0.75, \dots, 1.0(0.05)$ (from left to right). Inset: FS for $U/t = 10$ (solid) and $U = 0$ (dashed) for $2n_0 = 0.9, 1.0, 1.1$ (from left to right) in the lattice-symmetric phase.

but differ significantly for finite Φ . In contrast, for fixed n_0 , only the slope of the curves becomes smaller when we decrease U ; see the inset of Fig. 4.

For sufficiently large values of U/t and close to half band-filling, these Fermi surfaces are unstable against the Pomeranchuk effect [22–25], i.e., we find minima in the variational space which break the discrete C_4 symmetry of the lattice, in agreement with related numerical work on t - J models [26–28]. In Fig. 5 we show the FS for $2n_0 = 0.9, 0.95, 1.0$ for $U/t = 10$ (Pomeranchuk phases) and $U/t = 0$. Around half band-filling, $|2n_0 - 1| \lesssim 0.12$, the states with broken symmetry are stable. As seen from the inset of Fig. 5, the maximal energy gain due to the symmetry breaking is of a fraction of room temperature, $\Delta E/k_B \approx 100$ K for $t = 1.0$ eV.

The asymmetry of the Pomeranchuk FS at finite doping is quite remarkable. The two intersection points, denoted as k_x^1 and k_x^2 in Fig. 5, obey $k_x^1 = \pi - k_x^2$ only at half band-filling. The Pomeranchuk minima are not continuously connected to those without broken symmetries. Therefore, in our approach, the transitions between such states as a function of U/t are discontinuous, in general.

Second, we consider the Hubbard model with an additional second-neighbour hopping $t_{1,1} = -t' = 0.25t$. Even in the absence of symmetry breaking, the FS deformations are much larger than in the Hubbard model with nearest-neighbour hopping only, as seen from the inset of Fig. 6

where we show the lattice-symmetric FS for $U/t = 10$ and $U/t = 0$ near half band-filling. The Pomeranchuk instabilities occur mainly for hole doping, $0.70 \lesssim 2n_0 \lesssim 1.03$ for $U/t = 10$, see the inset of Fig. 5. In Fig. 6, we show the Pomeranchuk FS for $U/t = 10$ and the corresponding FS for $U/t = 0$ for densities $0.75 \leq 2n_0 \leq 1$.

Note that the results presented in Figs. 4-6 are certainly altered by the inclusion of other symmetry-broken phases with, e.g., magnetic or superconducting order. Such phases will be investigated in future studies. One should also keep in mind that our approach only allows us to study states which are adiabatically connected to some non-interacting reference system ('Fermi liquids'). This excludes, in particular, the investigation of Mott-Hubbard insulators. At zero temperature, however, such insulators are usually found only in theoretical studies which deliberately neglect ordered states, such as antiferromagnetic spin waves.

Conclusions. – In summary, we have introduced a novel scheme for the evaluation of Gutzwiller wave functions in finite dimensions. As a first application, we described the correlation-induced Fermi surface deformations in two-dimensional Hubbard models within the Gutzwiller approach. To the best of our knowledge, there exists no alternative method to calculate quasi-particle Fermi surfaces for interaction parameters $U \approx W$ in the Hubbard model. Our approach can be extended in various directions: to study magnetic and superconducting order in single and multi-band Hubbard models [29], and to calculate dynamical response functions [30–32].

REFERENCES

- [1] FETTER A. L. AND WALECKA J. D., *Quantum Theory of Many-Particle Systems* (Dover Publications, New York) 2003.
- [2] SCHWEITZER H. AND CZYCHOLL G., *Z. Phys. B*, **83** (1991) 93.
- [3] ZLATIĆ V., GRABOWSKI S. AND ENTEL P., *Phys. Rev. B*, **56** (1997) 14875.
- [4] HALBOTH C. J. AND METZNER W., *Z. Phys. B*, **102** (1997) 501.
- [5] HALBOTH C.J. AND METZNER W., *Phys. Rev. B*, **61** (2000) 125114.
- [6] FREIRE H., CORRERA E. AND FERRAZ A., *Phys. Rev. B*, **78** (2008) 125114.
- [7] BULUT N., SCALAPINO D. J. AND WHITE S. R., *Phys. Rev. B*, **50** (1994) 7215.
- [8] PREUSS R., HANKE W. AND VON DER LINDEN W., *Phys. Rev. Lett.*, **75** (1995) 1344.
- [9] EDER R., SEKI K. AND OHTA Y., *Phys. Rev. B*, **83** (2011) 205137.
- [10] VARNEY C. N., LEE C.-R., BAI Z. J., CHIESA S., JARRELL M. AND SCALETTAR R. T., *Phys. Rev. B*, **80** (2009) 075116.
- [11] GROS C., *Phys. Rev. B*, **38** (1988) 931.
- [12] YOKOYAMA H. AND SHIBA H., *J. Phys. Soc. Jpn.*, **57** (1988) 2482.
- [13] PARAMEKANTI A., RANDEKIA M. AND TRIVEDI N., *Phys. Rev. B*, **70** (2004) 054504.
- [14] EICHENBERGER D. AND BAERISWYL D., *Phys. Rev. B*, **76** (2007) 180504.
- [15] EICHENBERGER D. AND BAERISWYL D., *Phys. Rev. B*, **79** (2009) 100510.
- [16] GUTZWILLER M., *Phys. Rev. Lett.*, **10** (1963) 159.
- [17] GEBHARD F., *Phys. Rev. B*, **41** (1990) 9452.
- [18] METZNER W., *Z. Phys. B*, **77** (1989) 253.
- [19] METZNER W. AND VOLLHARDT D., *Phys. Rev. B*, **37** (1988) 7382.
- [20] KOLLAR M. AND VOLLHARDT D., *Phys. Rev. B*, **65** (2002) 155121.
- [21] GULÁCSI Z., GULÁCSI M. AND JANKÓ B., *Phys. Rev. B*, **47** (1993) 4168.
- [22] POMERANCHUK I. J., *JETP*, **8** (1958) 361.
- [23] HALBOTH C. J. AND METZNER W., *Phys. Rev. Lett.*, **85** (2000) 5162.
- [24] YAMASE H. AND KOHNO H., *J. Phys. Soc. Jpn.*, **69** (2000) 332.
- [25] YAMASE H. AND KOHNO H., *J. Phys. Soc. Jpn.*, **69** (2000) 2151.
- [26] EDEGGER B., GROS C. AND MUTHUKUMAR V. N., *Phys. Rev. B*, **74** (2006) 165109.
- [27] YAMASE H., *Phys. Rev. B*, **75** (2007) 014514.
- [28] JEDRAK J. AND SPALEK J., *Phys. Rev. B*, **81** (2010) 073108.
- [29] BÜNEMANN J., WEBER W. AND GEBHARD F., *Phys. Rev. B*, **57** (1998) 6896.
- [30] SEIBOLD G. AND LORENZANA J., *Phys. Rev. Lett.*, **86** (2001) 2605.
- [31] V. OELSEN E., SEIBOLD G. AND BÜNEMANN J., *Phys. Rev. Lett.*, **107** (2011) 076402.
- [32] V. OELSEN E., SEIBOLD G. AND BÜNEMANN J., *New J. Phys.*, **13** (2011) 113031.